

AperTO - Archivio Istituzionale Open Access dell'Università di Torino

Identifying the Role of Terahertz Vibrations in Metal-Organic Frameworks: From Gate-Opening Phenomenon to Shear-Driven Structural Destabilization

This is the author's manuscript

Original Citation:

Availability:

This version is available <http://hdl.handle.net/2318/157861> since 2016-08-04T13:21:12Z

Published version:

DOI:10.1103/PhysRevLett.113.215502

Terms of use:

Open Access

Anyone can freely access the full text of works made available as "Open Access". Works made available under a Creative Commons license can be used according to the terms and conditions of said license. Use of all other works requires consent of the right holder (author or publisher) if not exempted from copyright protection by the applicable law.

(Article begins on next page)

Supplemental Material

for

**Identifying the Role of Terahertz Vibrations in
Metal-Organic Frameworks: From Gate-Opening
Phenomenon to Shear-Driven Structural
Destabilization**

**Matthew R. Ryder,^{1,2,3} Bartolomeo Civalleri,⁴ Thomas D. Bennett,⁵
Sebastian Henke,⁵ Svemir Rudić,² Gianfelice Cinque,³ Felix Fernandez-
Alonso,^{2,6} and Jin-Chong Tan^{1*}**

¹*Department of Engineering Science, University of Oxford, Parks Road, Oxford OX1 3PJ, UK.*

²*ISIS Facility, Rutherford Appleton Laboratory, Chilton, Didcot OX11 0QX, UK.*

³*Diamond Light Source, Harwell Campus, Didcot, Oxford OX11 0DE, UK.*

⁴*Department of Chemistry, NIS and INSTM Reference Centre, University of Turin,
via P. Giuria 7, 10125 Torino, Italy.*

⁵*Department of Materials Science and Metallurgy, University of Cambridge, Cambridge CB3 0FS, UK.*

⁶*Department of Physics and Astronomy, University College London, Gower Street, London WC1E 6BT, UK.*

**Correspondence to: jin-chong.tan@eng.ox.ac.uk*

Table of Contents

1	Materials Synthesis and Characterization	3
2	Inelastic Neutron Scattering (INS).....	7
3	Synchrotron Radiation Far-Infrared (SR FIR) Absorption Spectroscopy.....	9
4	Vibrational Modes for Spectral Region $< 700 \text{ cm}^{-1}$ ($\sim 21 \text{ THz}$).....	10
5	<i>Ab Initio</i> Quantum Mechanical Simulations	11
5.1	DFT calculations of vibrational frequencies of periodic ZIF structures	11
5.2	Overtone associated with higher-order vibrational excitations	14
5.3	MP2 calculations to determine harmonic frequencies of imidazole molecules	16
6	Nature of THz Vibrational Modes $< 100 \text{ cm}^{-1}$ ($\sim 3 \text{ THz}$)	18
7	ZIF-4 Pore Modification Mechanisms Associated with THz Vibrations	21
8	Animations of ZIFs Lattice Dynamics	22
9	References	23

1 Materials Synthesis and Characterization

We have synthesized the ZIF-4 sample using a modified route from that reported in ref.[1], this was to ensure that a phase pure compound was obtained for this work. 1.2 g $\text{Zn}(\text{NO}_3)_2 \cdot 6\text{H}_2\text{O}$ and 0.9 g imidazole were dissolved in 90 mL DMF. The mixture was transferred into a 100 mL screw jar and tightly secured. The mixture was heated to 100°C for 3 days. After cooling the ZIF-4 crystals were filtered off, then washed 3 times with ~20 mL DMF and repeated 3 times with 20 mL DCM before air drying. Guest-free samples were prepared by immersing the dried crystals in 100 mL DCM and stirred gently for 3 days. Every 24 hours, the material was filtered off and the DCM was exchanged with 100 mL of fresh solvent. After the final filtering step, the sample was dried overnight in a vacuum oven at 120°C.

The ZIF-7 sample (i.e. ZIF-7-I [2]) was synthesized according to procedures reported by Park *et al.* [3]. The as-synthesized ZIF-7 was dried in the vacuum oven at room temperature overnight, and without further activation step to prevent (unwanted) phase transition from ZIF-7-I to ZIF-7-II [2]. Using FTIR spectroscopy (Fig. S3), we have established that the ZIF-7 sample contains DMF (*N,N*-dimethylformamide) solvent molecules used for synthesis, which is key to retaining the ZIF-7-I phase. We note that, recently Zhao *et al.* [2] reported heating of ZIF-7-I in vacuum at 77°C will yield ZIF-7-II due to the removal of entrapped DMF.

ZIF-8 sample was synthesized according to procedures reported in the literature [3, 4]. The activation of ZIF-8 was performed by solvent-exchange in methanol overnight followed by evacuation for 24 hours at room temperature, and finally the sample was dried overnight in a vacuum oven at 150°C.

Prior to the inelastic neutron scattering and synchrotron far-infrared spectroscopic experiments, the purity and crystallinity of the powdered samples were confirmed using powder X-ray diffraction (PXRD) on a Bruker D8 diffractometer, using Cu K_α radiation ($\lambda = 1.5418 \text{ \AA}$) together with a LynxEye position-sensitive detector in the Bragg-Brentano geometry. All measurements were performed at ambient condition in the 2θ range of 5° to 50°. The PXRD patterns of ZIFs-4, -7, -8 are shown below.

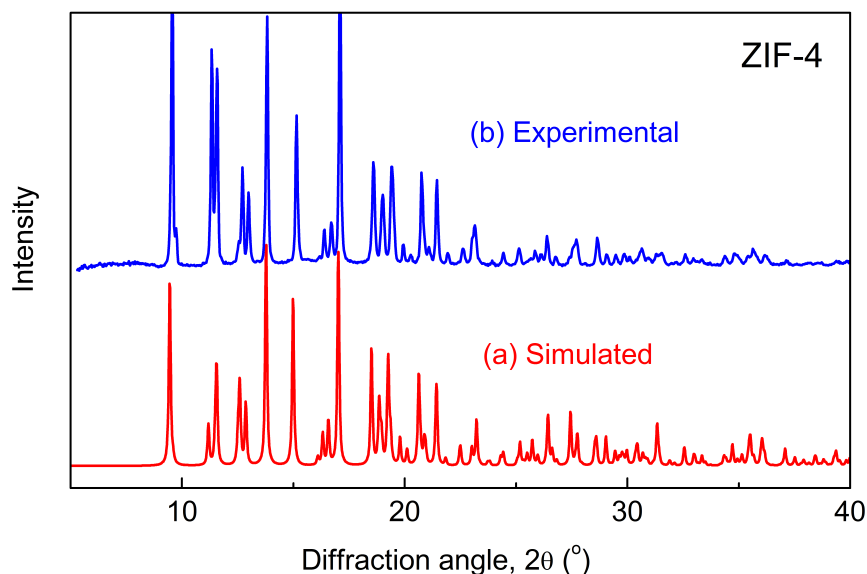


Fig. S1. PXRD of ZIF-4. Simulated pattern using crystal structure deposited by Park *et al.* [3] (CCDC code: VEJYUF [5]). (b) Activated sample used in this work.

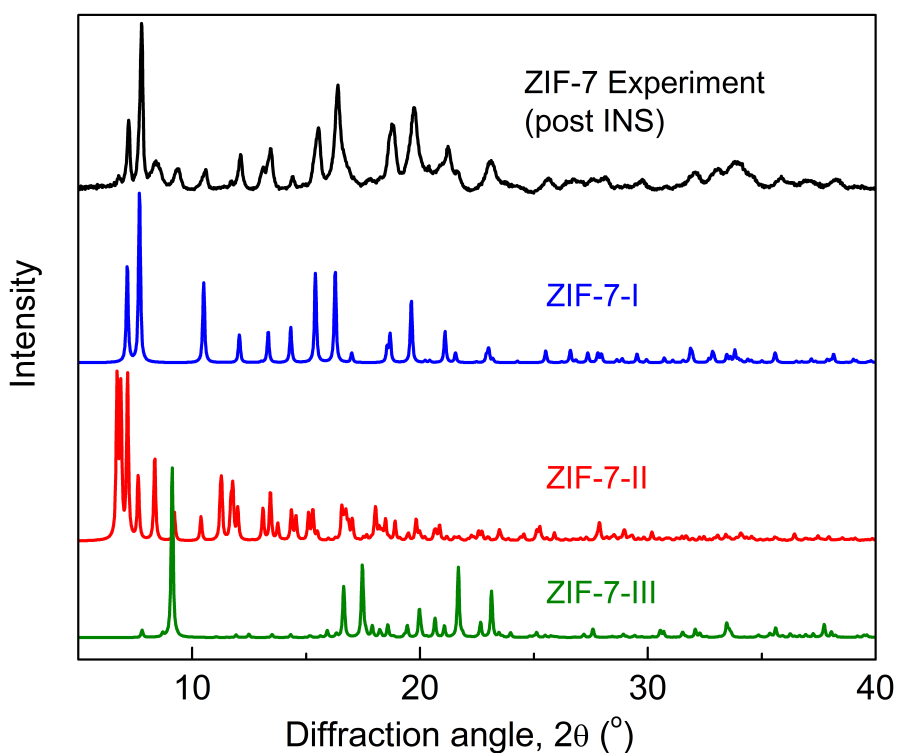


Fig. S2. PXRD of ZIF-7 sample used in this study (black curve), this diffraction pattern was collected using powders that have been subjected to inelastic neutron scattering (INS). Our ZIF-7 sample matches the simulated pattern of ZIF-7-I phase (blue), which is significantly different from two other recently reported phases [2]: ZIF-7-II (red) and ZIF-7-III (green). Simulated pattern of ZIF-7-I was generated using crystal structure

deposited by Park *et al.* [3] (CCDC code: VELVIS [5]), while those of ZIF-7-II and ZIF-7-III based on crystal structures reported by Zhao *et al.* [2]

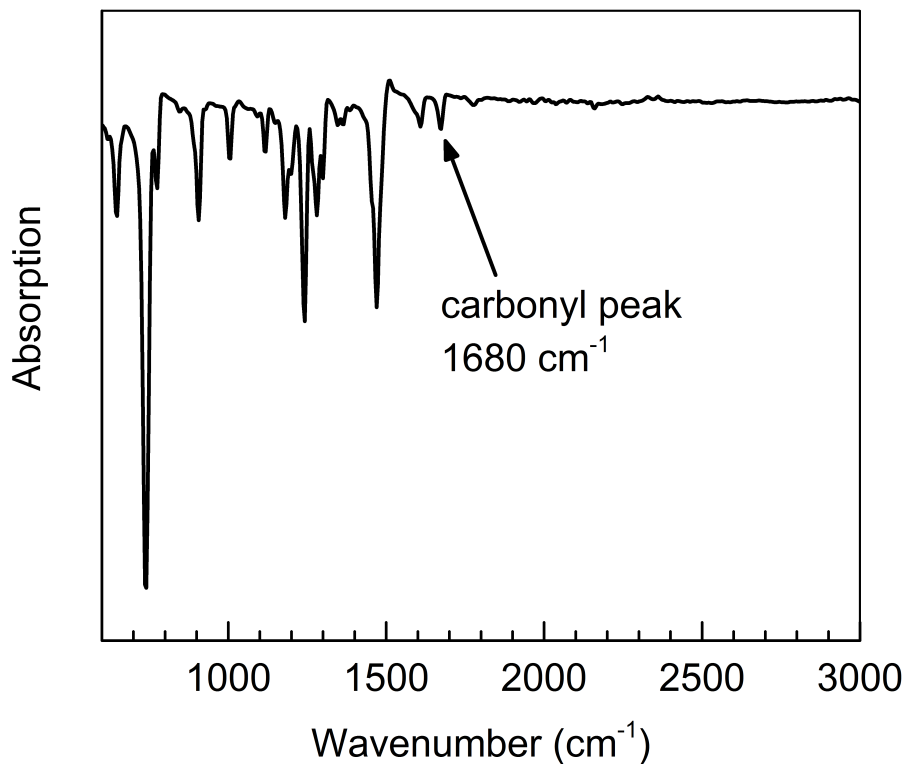


Fig. S3. FTIR spectra of the ZIF-7 sample (retrieved after INS experiment, see Fig.S2). The presence of the carbonyl peak (amides) confirms that the pores of the framework contain DMF solvents.

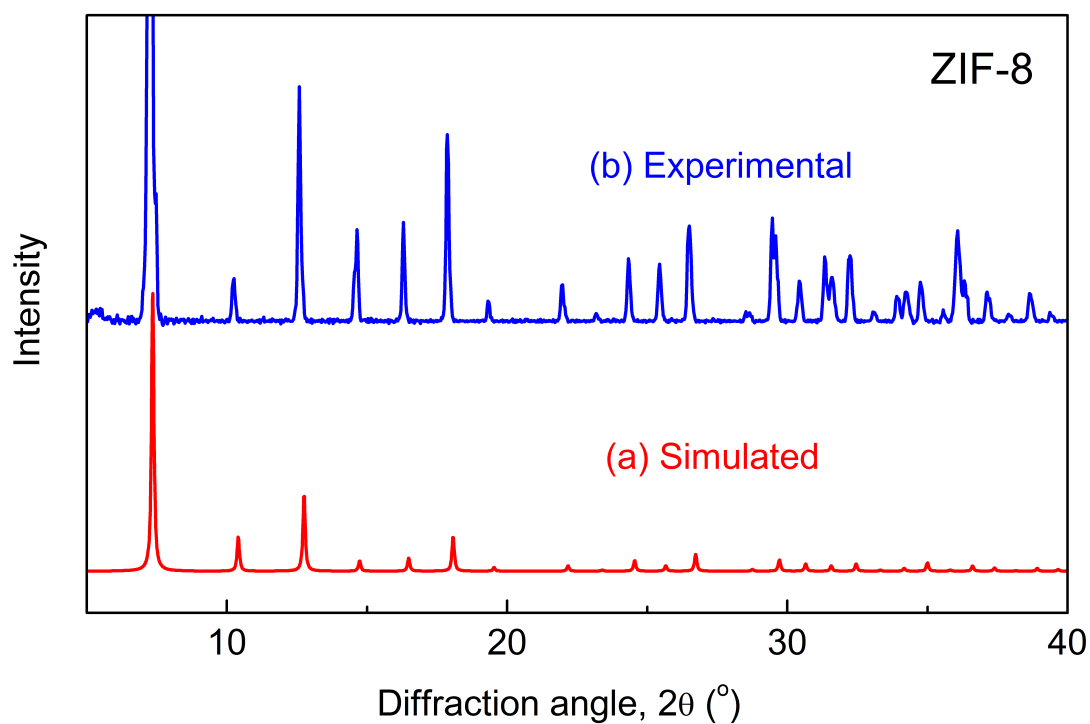


Fig. S4. PXRD of ZIF-8. (a) Simulated pattern using crystal structure deposited by Moggach *et al.* [6] (CCDC code: TUDKEJ [5]). (b) Activated sample used in this work.

2 Inelastic Neutron Scattering (INS)

The INS spectra were recorded using the high resolution ($\Delta E/E \sim 1.25\%$) broadband ($-24 - 4000 \text{ cm}^{-1}$) TOSCA spectrometer [7-9] at the ISIS Pulsed Neutron and Muon Source of the Rutherford Appleton Laboratory (Chilton, UK). TOSCA is an indirect geometry time-of-flight spectrometer where a pulsed, polychromatic beam of neutrons illuminates the sample at a distance of 17 m from the source (room temperature water moderator).

Energy analysis was performed after the interaction of the incident neutron beam with the sample under investigation. The sample scattered neutrons were Bragg reflected by a pyrolytic graphite analyser, while higher-order reflections beyond (002) were suppressed by a cooled ($T < 50 \text{ K}$) Beryllium (Be) filter so as to define a unique final energy. Thus neutrons with a final energy of approximately 32 cm^{-1} were passed towards the ^3He detector bank. The detector array was comprised of a total of ten banks each having thirteen ^3He tubes with an effective length (thickness) of 250 (2.5) mm. Five banks were located in forward scattering (scattering angle $\sim 45^\circ$) and five in backscattering ($\sim 135^\circ$) direction. The use of a low (fixed) final energy translated into a direct relationship between energy transfer ($E_T, \text{ cm}^{-1}$) and momentum transfer ($Q, \text{ \AA}^{-1}$) such that $E_T \approx 16Q^2$. Energy transfer and spectral intensity were then calculated using standard programs to convert to the conventional $S(Q, \omega)$.

A disc chopper to prevent frame overlap was positioned at 8 m from the moderator. It relied on the 40 ms timeframe during the operation of both target stations at ISIS to extend the incident-wavelength bandwidth of the instrument down to -24 cm^{-1} i.e. elastic line region. The samples (2–3 g) were wrapped in $4 \times 4 \text{ cm}$ aluminium foil sachets (which filled the neutron beam at the sample position) and placed in thin walled aluminium cans. To reduce the impact of the Debye–Waller factor on the observed spectral intensity, the samples i.e. the sample chamber was cooled to approximately 10 K by a closed cycle refrigerator (CCR) and the spectra were recorded for 6 to 12 hours.

TOSCA outstanding spectral resolution (*ca.* $1.25\% E_T$), arises from the combination of several factors: the narrow bandpass of the PG002/Be analyser, tight moderator pulse widths ($\sim 10 \text{ \mu s/\AA}$), a long incident flight path and a time- and energy-focused detector

geometry. Quantitatively, the above design choices translate into an absolute spectral resolution of $\sim 2.4 \text{ cm}^{-1}$ for elastic events ($E_T = 0 \text{ cm}^{-1}$) and $\sim 50 \text{ cm}^{-1}$ at $E_T = 4000 \text{ cm}^{-1}$. Instrument backgrounds are negligible, thus low-cross section measurements beyond hydrogen-containing materials are not only feasible but also a growing area of research on the instrument.

3 Synchrotron Radiation Far-Infrared (SR FIR) Absorption Spectroscopy

Infrared (IR) absorption spectra of all compounds were recorded at the Multimode InfraRed Imaging and Microspectroscopy (MIRIAM) Beamline B22 located in the Diamond Light Source synchrotron [10]. The great advantage of the synchrotron radiation (SR) IR source was mainly the brightness of the beam (photon flux density several order of magnitude higher than conventional sources) and broadband spectral range (covering simultaneously from the visible to the sub-THz region). The storage ring was operating in the standard user mode, i.e. 900 bunches filling pattern for a total circulating current of 300 mA and top up at every 10 minutes (lifetime circa 18 h and photon flux fluctuation limited to 0.3%). IR spectroscopy was performed in vacuum via a Bruker Vertex 80 V Fourier Transform IR (FTIR) interferometer (Bruker Optics, Ettlingen, Germany) equipped with an RT DLaDTGS detector. The measurements were performed at a resolution of 1 cm^{-1} with a $6\text{ }\mu\text{m}$ thick Mylar broad-band multilayer beamsplitter (allowing the spectral range below 700 cm^{-1}) at a scanner velocity of 10 kHz (with respect to the $15,800\text{ cm}^{-1}$ laser reference).

The experiments were performed at room temperature (RT) using the Attenuated Total Reflection (ATR) method for the advantage of measuring samples without any preparation [11]. Specifically, the MOF powder was placed on top of a diamond ATR crystal into a Bruker Diamond ATR accessory, and the sample was held in position by pressure applied onto a HDPE disk *via* a clamp mechanism. Schematically, the synchrotron IR beam enters the ATR crystal from the bottom at an angle of circa 45° to be totally reflected at the crystal-sample interface, then re-directed *via* a circa 45° mirror to the detector pupil. Provided the sample refractive index is lower than the ATR material (diamond $n = 2.4$) only a fraction of radiation reaches into the sample (evanescent wave). At the wavelength where the sample absorbs energy the evanescent wave will be attenuated, and consequently the beam exiting is modulated like in a transmission measurement. The beam penetration depth in ATR mode depends linearly on the wavelength (for diamond and the geometry used this penetration is below 2 mm for soft materials), plus the ATR spectrum is influenced by the relative refractive index change of the sample. For these reasons the spectra shown have been corrected via Extended ATR correction algorithms in the OPUS 7.2 software used for data acquisition and subsequent analysis.

4 Vibrational Modes for Spectral Region < 700 cm⁻¹ (~21 THz)

Table S1: Assignment of vibrational modes up to 87 meV, based on DFT calculations (§5).

ZIF- <i>n</i>	Wavenumber (cm ⁻¹)	Energy Loss (meV)	Description of vibrational motions
ZIF-4	<100	<12.4	See Table S3
	100-185	12.4-22.9	4-Membered and 6-Membered Ring Deformation; Ligand Rotation (Rocking)
	185-275	22.9-34.1	N-Zn-N Bending and Zn-N Stretching (Tetrahedral Deformation); Ligand Rotation (Rocking)
	285-325	35.3-40.3	Zn-N Stretching (Belonging to ZnN ₄ Tetrahedra)
	640-700+	79.3-86.8	Aromatic Ring Deformation (In-Plane and Out-of-Plane)
ZIF-7	<100	<12.4	See Table S3
	100-150	12.4-18.6	4-Membered and 6-Membered Ring Deformation; Ligand Rocking
	150-225	18.6-27.9	N-Zn-N Bending and Zn-N Stretching (Tetrahedral Deformation) (Due to the symmetry of the mode at 153.8 cm ⁻¹ it results in 6-membered ring breathing/pore expansion)
	225-245	27.9-30.4	Bending at the Bridge of the Aromatic Rings (Due to the symmetry of the mode at 234.3 cm ⁻¹ it results in 6-membered ring gate opening)
	275-290	34.1-36	Zn-N Stretching
	295-315	36.6-39.1	Ligand Twisting (Torsion)
	420-430	52.1-53.3	Phenyl Ring Distortion (Ring Flapping/Wagging)
	460-470	57-58.3	Ligand Bending (Zn-N-C and N-C*-C) *Ring Bridging
	545-700+	67.6-86.8+	Aromatic Ring Deformation (In-Plane and Out-of-Plane)
ZIF-8	<100	<12.4	See Table S3
	100-195	12.4-24.2	4-Membered and 6-Membered Ring Deformation; Ligand Rotation (Rocking) (Due to the symmetry of the mode at 101.1 cm ⁻¹ it results in 4MR gate opening, 126.3 cm ⁻¹ results in 4MR and 6MR gate opening and 131.3 cm ⁻¹ results in 4MR gate opening)
	195-245	24.2-30.4	N-Zn-N Bending and Zn-N Stretching (Tetrahedral Deformation)
	260-270	32.2-33.5	Ligand Bending (Methyl Group Out-of-Plane Rocking)
	280-305	34.7-37.8	Zn-N Stretching
	415-425	51.5-52.7	Ligand Bending (Zn-N-C and N-C-Me)
	638-700+	79.1-86.8+	Aromatic Ring Deformation (In-Plane and Out-of-Plane)

5 *Ab Initio* Quantum Mechanical Simulations

5.1 DFT calculations of vibrational frequencies of periodic ZIF structures

Density functional theory (DFT) calculations were carried out at the PBE [12] level of theory augmented with a damped empirical dispersion term (PBE-D) [13] and performed with the periodic *ab initio* code CRYSTAL14 [14]. Crystalline orbitals were represented as linear combinations of Bloch functions (BF), and were evaluated over a regular three-dimensional (3D) mesh in reciprocal space. Each BF was constructed from local atomic orbitals (AOs), which are linear combinations (with constant coefficients) of Gaussian-type functions (GTFs). Each GTF is the result of a Gaussian multiplied by a solid spherical harmonic.

All electron TZVP basis sets were used for Zn, N, C and H atoms, consistent with our previous work on ZIF-8 [15]. The adopted basis sets contain 4352, 2736 and 2016 basis functions for ZIF-4, ZIF-7 and ZIF-8, respectively. For the exact basis sets used in this study, please see other supplemental information (filename: BasisSets-Ryder-PRL.txt).

A full relaxation of both lattice parameters and atomic coordinates was allowed. The geometry optimisation at constant symmetry was performed by means of a quasi-Newtonian algorithm in which the quadratic step (BFGS Hessian updating scheme) is combined with a linear one (parabolic fit) as proposed by Schlegel [16-20]. Convergence was tested on the root mean square (RMS) and the absolute value of the largest component of the gradients and the estimated displacements. The threshold for the maximum and RMS gradient, and the maximum and RMS atomic displacement of all atoms was set to 1.5×10^{-4} , 1.0×10^{-4} , 3.0×10^{-4} and 2.0×10^{-4} a.u., respectively. The optimisation was considered to have completed when all four conditions were simultaneously satisfied.

The mass-weighted Hessian matrix for the calculation of the vibrational frequencies was obtained by numerical differentiation of the analytical first derivatives, calculated at geometries obtained by slightly displacing in turn each of the $3N$ nuclear coordinates with

respect to the equilibrium geometry. Vibrational frequencies were calculated at the Γ point, as the volume of each system is sufficient to expect negligible phonon dispersion.

The IR intensities were calculated through the Berry Phase approach [21], by evaluating the atomic Born tensors as polarization differences between the original and the distorted geometries. This approach assumes the polarization difference is equal to the time-integrated transient macroscopic current that flows through the sample during the vibrations.[14, 22]

Summarized below are the comparisons of lattice parameters calculated from DFT (for ideal crystalline structures) versus experimental values reported in literature.

ZIF-4 (<i>Pbca</i>)				
<i>Method</i>	<i>Lattice parameters (Å)</i>			<i>Volume (Å³)</i>
	<i>a</i>	<i>b</i>	<i>c</i>	
[†] Experimental CIF (Refcode VEJYUF [5])	15.395	15.307	18.426	4342.11
PBE-D	15.423	15.344	18.618	4405.96
<ul style="list-style-type: none"> • Average error in lattice parameters: 0.49% 				

ZIF-7 (<i>R-3</i>)			
<i>Method</i>	<i>Lattice parameters (Å)</i>		<i>Volume (Å³)</i>
	<i>a</i>	<i>c</i>	
[†] Experimental CIF (Refcode VELVIS [5])	22.989	15.763	7214.56
PBE	23.258	16.069	7528.52
PBE-D	21.382	16.416	6499.53
<ul style="list-style-type: none"> • Average error in lattice parameters using PBE is 1.56%. We note the error is relatively higher for PBE-D (5.57%) due to dispersion correction overestimating the interactions caused by extended aromaticity of the bulky benzimidazolate ligands. Fig. S5 shows that the predicted vibrational spectra are consistent with experiments. 			

ZIF-8 (<i>I-43m</i>)				
<i>Method</i>	<i>Lattice parameters (Å)</i>			<i>Volume (Å³)</i>
	<i>a</i>	<i>b</i>	<i>c</i>	
[‡] Experimental CIF (Refcode TUDKEJ [5])	16.992	16.992	16.992	4906.07
◊PBE-D	16.867	16.951	17.164	4907.40
<ul style="list-style-type: none"> • Average error in lattice parameters: 0.66% 				

Notes:

- †Crystallographic information file (CIF) deposited to CCDC [5] by ref.[3], in which single-crystal XRD data were collected at 283(2) K.
- ‡Experimental cell parameters of ZIF-8 determined from (i) single-crystal X-ray diffraction [6]: $a = 16.9920(8)$ Å at 293 K, (ii) neutron powder diffraction [23]: $a = 16.9900(2)$ Å at 3.5 K and $a = 17.0117(4)$ at 200 K.
- ◇Symmetry lowered in DFT optimization of ZIF-8, due to imaginary frequencies being present when using the experimentally assigned space group (293 K). The imaginary modes can be linked to the rotation of the methyl groups observed at low temperatures (see ref.[23]). To account for this effect, the symmetry of the system was relaxed to allow for a stable structure with minimum potential energy to be optimized.

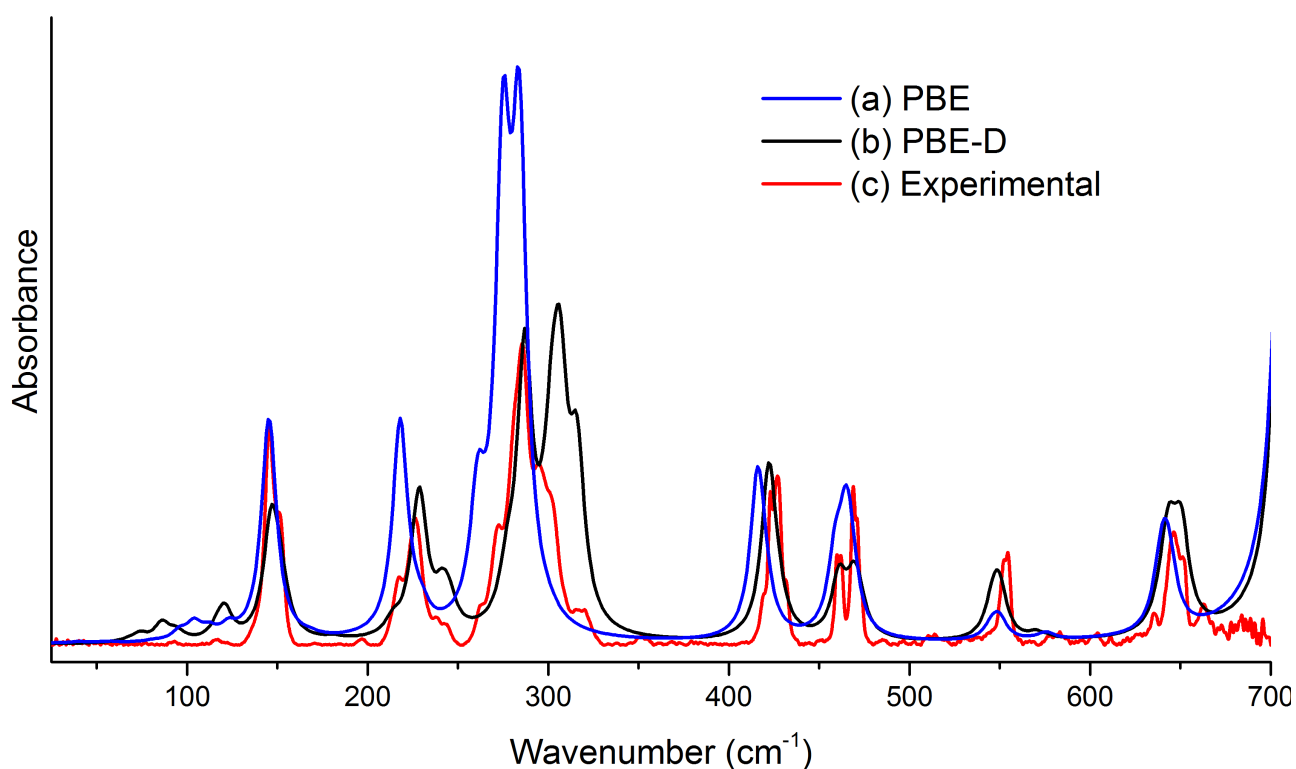


Fig. S5. Comparison of far-IR spectra in the region of 25-700 cm^{-1} between (a) DFT PBE, (b) DFT PBE-D and (c) synchrotron radiation FIR measurements.

5.2 Overtones associated with higher-order vibrational excitations

The theoretical results place the highest peaks at 3196, 3180 and 3195 cm^{-1} for ZIF-4, ZIF-7 and ZIF-8 respectively. In reality, however, the experimental spectrum is more complex (see Fig.2 in main manuscript), as higher orders of vibrational excitation take place and even though the probability is far less, the collective contribution to the spectral results is significant. It is, therefore, necessary to include in the theoretical results the overtones that would be expected from these excitations, which was achieved using the vibrational eigenvectors, generated from the DFT calculations, with the aClimax code [24, 25]. The theoretical spectra include up to 10th order overtones with fully anisotropic external Debye-Waller effects. This approximation of the probability of higher order excitations has allowed for the theoretical results to match exceptionally well with that of experiment. To account for the overtone peaks being shifted to higher regions, we have shown each spectra up to 4000 cm^{-1} .

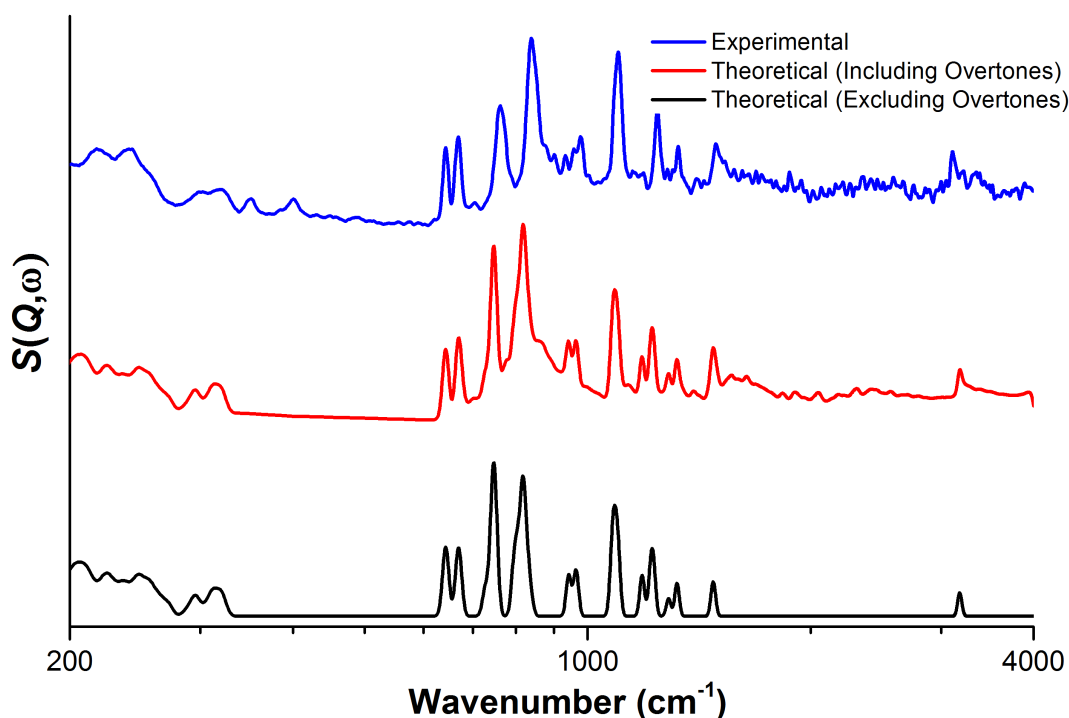


Fig. S6. Comparison of DFT spectra, for ZIF-4, with and without the inclusion of higher order vibrational excitations.

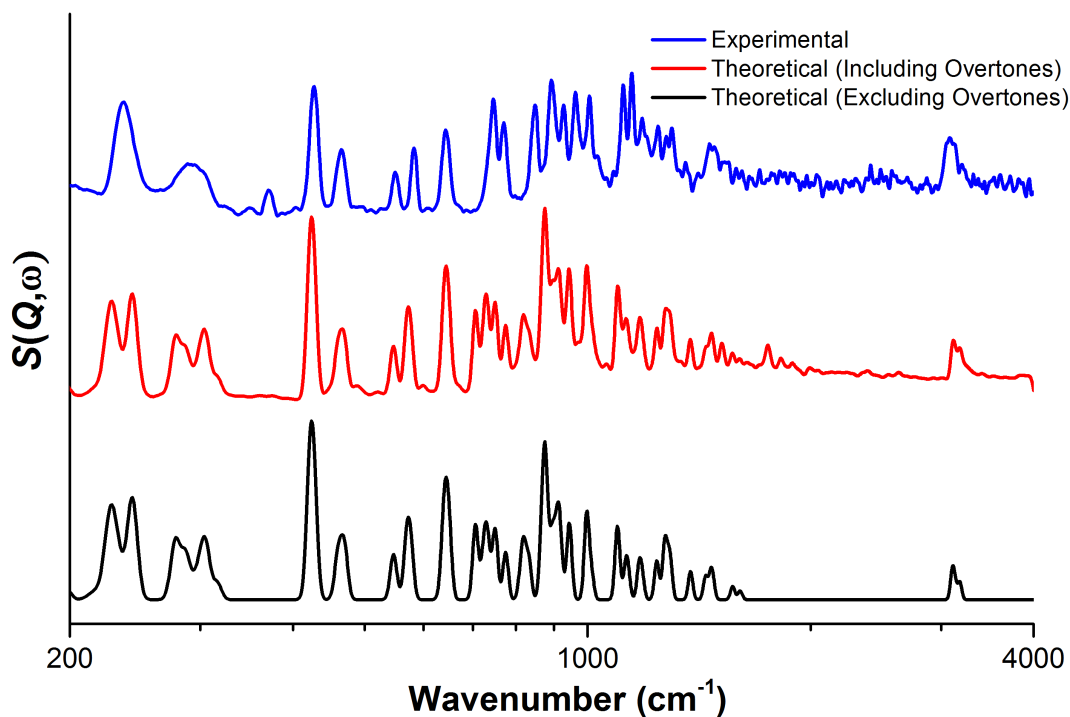


Fig. S7. Comparison of DFT spectra, for ZIF-7, with and without the inclusion of higher order vibrational excitations.

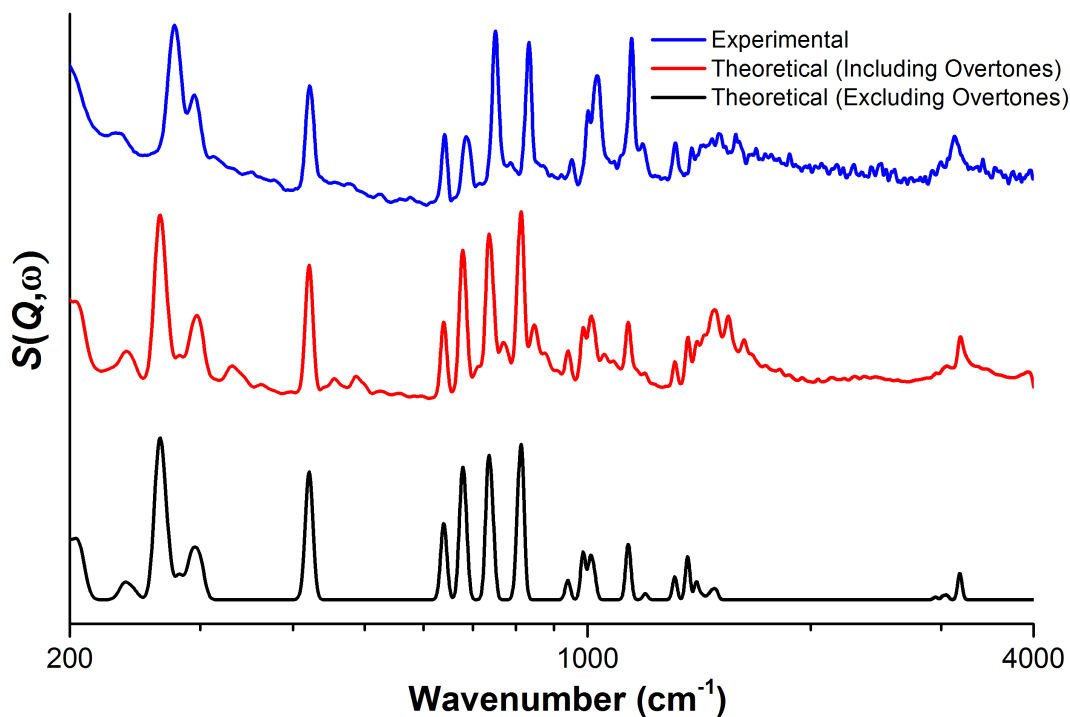


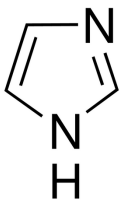
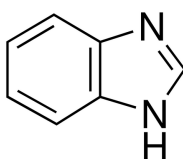
Fig. S8. Comparison of DFT spectra, for ZIF-8, with and without the inclusion of higher order vibrational excitations.

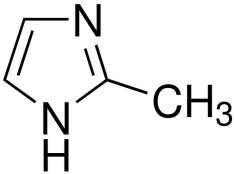
5.3 MP2 calculations to determine harmonic frequencies of imidazole molecules

To further pinpoint the exact nature of the vibrational modes, we calculated the theoretical spectra of the isolated gas-phase molecules that constitute the organic bridging linkers in each framework. The minimum energy structure and harmonic frequency calculations for the three individual organic linker molecules: Imidazole (Im), benzimidazole (blm), and 2-methylimidazole (mlm), were carried out with the Gaussian 09 code [26]. The calculations were performed at the MP2 [27] level of theory with the aug-cc-pVDZ [28] basis set.

The predictions obtained are tabulated in Table S2 below, which are found to be consistent with spectroscopic measurements available in the literature, see for example [29-31]. Vibrational signatures of the isolated molecular systems enabled us to confirm that, the major vibrational modes of ZIFs are indeed those that involved a contribution from the inorganic building units, i.e. ZnN_4 tetrahedra. On this basis, certain modes corresponding to organic linker vibrations are being shifted to lower energy levels upon formation of 3-D extended frameworks.

Table S2: Theoretical IR-active vibrational modes of the imidazole-based molecules.

Organic Linker (Ligand)	Energy band (cm ⁻¹)	Description of vibrational modes
Imidazolate (Im) 	550, 644, 680, 735, 819, 868	Out-of-Plane Ring Deformation
	903, 940	In-Plane Ring Deformation
	1070, 1090, 1138, 1164, 1275, 1365, 1435, 1495, 1553	C-C/C-N Stretch and C-H Bend
	3250, 3254	Asymmetric C-H Stretch
	3280	Symmetric C-H Stretch
	3650	N-H Stretch
Benzimidazole (blm) 	226	Bend at the Bridging of the Rings
	256	Asymmetric Ring Rotation
	416	N-C*-C Bend (* Ring Bridging)
	434	Phenyl Ring Deformation (Wing Flapping)
	475, 549, 594, 627, 651, 750, 788, 790, 857, 874, 884, 944, 945, 988	In-plane and Out-of-plane Ring Deformation

	1025, 1092, 1124, 1161, 1198, 1268, 1283, 1330, 1383, 1419, 1471, 1515, 1529, 1624, 1663	C-C/C-N Stretch and C-H Bend
	3174, 3182, 3194	Asymmetric C-H Stretch of Phenyl Ring
	3203	Symmetric C-H Stretch of Phenyl Ring
	3242	C-H Stretch of Im Ring
	3653	N-H Stretch
	70	Methyl Rotation
	253	Out-of-Plane Me-Im Bend
	349	In-Plane Me-C-N Bend
2-Methylimidazole (mlm)	543, 641, 678, 690, 728, 859, 926, 963, 1001, 1050, 1093, 1131, 1179, 1270, 1378, 1403, 1427, 1459, 1482, 1513, 1593	In-plane and Out-of-plane Ring Deformation
	3027	Symmetric C-H Stretch of Methyl Group
	3079, 3146	Asymmetric C-H Stretch of Methyl Group
	3248	Asymmetric C-H Stretch of Im Ring
	3278	Symmetric C-H Stretch of Im Ring
	3645	N-H Stretch

6 Nature of THz Vibrational Modes < 100 cm⁻¹ (~3 THz)

Table S3: Assignment of the THz vibrational modes obtained from DFT calculations in §5.

ZIF-n	Wavenumber (cm ⁻¹)	Band (THz)	Activity	Distinct characteristics of the vibrational motions
ZIF-4	6.98	0.21	Raman	Strong 4-Membered Ring Shearing and Strong 6-Membered Ring Deformation (Phase Transition)
	14.40, 14.50, 17.96	0.43, 0.43, 0.54	Raman	4-Membered Ring Shearing and 6-Membered Ring Deformation
	18.36, 20.47	0.55, 0.61	Raman	Strong 6-Membered and 4-Membered Ring Deformations
	21.29, 21.89	0.64, 0.66	IR	
	22.55	0.68	Raman	
	23.34	0.70	IR	
	26.65, 26.84, 27.04, 30.84	0.80, 0.80, 0.81, 0.92	Raman	
	33.06	0.99	Raman	
	33.08, 33.51	0.99, 1.00	IR	
	33.95	1.02	Raman	
	34.87	1.05	IR	
	35.13, 37.70	1.05, 1.13	Raman	
	40.57	1.22	IR	
	41.12, 41.19, 43.20, 45.61, 47.28	1.23, 1.24, 1.30, 1.37, 1.42	Raman	
	47.71	1.43	IR	
	49.62, 49.77	1.49, 1.49	Raman	
	52.25, 53.68	1.57, 1.61	IR	
	53.93	1.62	Raman	
	55.26, 55.56	1.66, 1.67	IR	
	57.96, 58.01, 58.74	1.74, 1.74, 1.76	Raman	
	62.01, 63.65	1.86, 1.91	IR	
	63.74, 64.30	1.91, 1.93	Raman	
	64.74	1.94	IR	
	65.02, 65.92, 67.97, 68.57, 69.71	1.95, 1.98, 2.01, 2.06, 2.09	Raman	
	69.91	2.10	IR	
	70.67, 70.82	2.12, 2.12	Raman	
	71.41, 71.74	2.14, 2.15	IR	
	73.60, 74.07	2.21, 2.22	Raman	
	76.83	2.30	IR	
	79.50	2.38	Raman	
	80.48	2.41	IR	
	81.14, 83.13	2.43, 2.49	Raman	
	83.14	2.49	IR	
83.82, 85.67	2.51, 2.57	Raman		
88.54, 88.97	2.65, 2.67	IR		
91.55, 93.93, 94.50, 95.51, 97.05	2.74, 2.82, 2.83, 2.86, 2.91	Raman		
97.21, 97.80	2.91, 2.93	IR		
98.86	2.96	Raman		
99.15	2.97	IR		
99.71, 99.77	2.99, 2.99	Raman		

ZIF-n	Wavenumber (cm ⁻¹)	Band (THz)	Activity	Distinct characteristics of the vibrational motions
ZIF-7	21.76, 21.76	0.65	Raman	6-Membered Ring Deformation (Phase Transition); 4-Membered Ring Rotation
	21.81	0.65	Raman	Strong 6-Membered Ring Rotational Expansion (Breathing); 4-Membered Ring Shearing induced Breathing
	25.00, 25.00	0.75, 0.75	IR	Strong Asymmetric Ligand Flapping/Wagging
	31.56	0.95	IR	Strong 6-Membered and 4-Membered Ring Deformation
	38.73	1.16	Raman	Low-amplitude (weak) 6-Membered Ring Rotational Expansion (Breathing); 4-Membered Ring Shearing
	38.77, 38.77	1.16, 1.16	Raman	Strong 6-Membered Ring Deformation; 4-Membered Ring Deformation; Asymmetric Ligand Flapping/Wagging
	48.56	1.46	IR	6-Membered Ring Deformation; Light 4-Membered Ring Deformation; Asymmetric Ligand Flapping/Wagging
	48.99	1.47	Raman	Strong Symmetric Ligand Flapping/Wagging (Gate Opening)
	55.77, 55.77	1.67, 1.67	Raman	6-Membered and 4-Membered Ring Deformation
	56.48, 56.48	1.69, 1.69	IR	6-Membered and 4-Membered Ring Deformation
	60.22	1.81	Raman	Light 6-Membered Ring Translational Expansion (Breathing); 4-Membered Ring Rocking
	61.74	1.85	IR	Light 6-Membered Deformation; Ligand Rocking
	65.06, 65.06	1.95, 1.95	Raman	6-Membered and 4-Membered Ring Deformation
	66.94	2.01	Raman	Strong 6-Membered and 4-Membered Ring Expansion (Breathing)
	68.23, 68.23	2.05, 2.05	IR	Light 6-Membered Deformation; Ligand Rocking
	74.16, 74.16	2.22, 2.22	Raman	Light 6-Membered and 4-Membered Ring Deformation; Ligand Rocking
	74.16, 74.16, 78.34	2.22, 2.22, 2.35	IR	Light 6-Membered and 4-Membered Ring Rocking; Ligand Rocking
	78.49	2.35	Raman	6-Membered and 4-Membered Ring Rocking; Ligand Rocking
	85.20, 85.20	2.55, 2.55	Raman	6-Membered Ring Deformation; Ligand Rocking
	85.93	2.58	IR	Strong 6-Membered Ring Deformation; 4-Membered Ring Rocking
	87.44, 87.44	2.62, 2.62	IR	6-Membered and 4-Membered Ring Deformation; Ligand Rocking
	92.95	2.79	IR	Light 6-Membered Ring Deformation; 4-Membered Ring Rocking; Strong Ligand Rocking
	94.26, 94.26	2.83, 2.62	IR	6-Membered Ring Deformation; 4-Membered Ring Rocking; Ligand Rocking
96.57	2.90	IR	6-Membered Ring Deformation; 4-Membered Ring Rocking	
97.19	2.91	Raman	Ligand Rocking with 6-Membered Ring Rotational Expansion (Breathing); 4-Membered Ring Deformation	

ZIF-n	Wavenumber (cm ⁻¹)	Band (THz)	Activity	Distinct characteristics of the vibrational motions
ZIF-8	18.38, 18.94, 20.08	0.55, 0.57, 0.60	IR	6-Membered Ring Deformation (Phase Transition); 4-Membered Ring Rotation; Methyl Group Rotation
	21.84	0.65	Raman	6-Membered Ring Rotation; 4-Membered Ring Shearing; Methyl Group Rotation
	30.81	0.92	Raman	Symmetric 4-Membered Ring Gate Opening with Strong Methyl Rotation Blocking Open Gates
	33.36	1.00	Raman	Symmetric 4-Membered Ring Gate Opening
	33.39, 34.73, 37.38	1.00, 1.04, 1.12	IR	Ligand Rocking (Asymmetric Gate Opening) and Methyl Group Rotation
	42.73	1.28	Raman	4-Membered Ring Deformation (Some Gate Opening/Breathing); Strong Methyl Group Rotation
	46.73, 47.20, 47.93	1.40, 1.41, 1.44	IR	6-Membered and Strong 4-Membered Ring Deformation (Some Gate Opening/Breathing); Strong Methyl Group Rotation
	53.05, 54.10, 55.35	1.59, 1.62, 1.66	IR	6-Membered and Strong 4-Membered Ring Deformation; Methyl Group Rotation
	60.19, 60.77, 60.78	1.80, 1.82, 1.82	IR	6-Membered and 4-Membered Ring Deformation; Methyl Group Rotation
	61.92, 64.25	1.86, 1.93	IR	6-Membered and 4-Membered Ring Deformation
	64.44	1.93	IR	6-Membered and 4-Membered Ring Deformation; Strong Methyl Group Rotation
	64.61	1.94	Raman	Light 4-Membered Ring Shearing; Strong Methyl Group Rotation
	65.55	1.97	IR	6-Membered and 4-Membered Ring Deformation; Light Methyl Group Rotation
	67.10, 69.75	2.01, 2.09	IR	Ligand Rocking and Strong Methyl Group Rotation
	75.32	2.26	Raman	Ligand Rocking and Methyl Group Rotation; Light 4-Membered Ring Breathing
	77.05, 77.31	2.31, 2.32	IR	Ligand Rocking and Methyl Group Rotation; Light 6-Membered Ring Deformation
	78.55	2.35	Raman	Ligand Rocking and Methyl Group Rotation
	79.57, 79.99, 80.27	2.39, 2.40, 2.41	IR	6-Membered and 4-Membered Ring Deformation; Strong Methyl Group Rotation
	81.38, 82.44	2.44, 2.47	IR	6-Membered and 4-Membered Ring Deformation; Light Methyl Group Rotation
	82.86, 83.71	2.48, 2.51	IR	Ligand Rocking and Methyl Group Rotation
	94.22	2.82	Raman	6-Membered Ring Deformation; 4-Membered Ring Breathing (Cage Opening)
	94.90, 95.45	2.84, 2.86	IR	6-Membered and 4-Membered Ring Deformation
	96.20, 96.75, 96.77	2.88, 2.90, 2.90	IR	6-Membered Ring Expansion; 4-Membered Ring Deformation
97.84	2.93	Raman	Ligand rocking; 4-Membered Ring Breathing	
98.56	2.95	IR	6-Membered and 4-Membered Ring Deformation	

7 ZIF-4 Pore Modification Mechanisms Associated with THz Vibrations

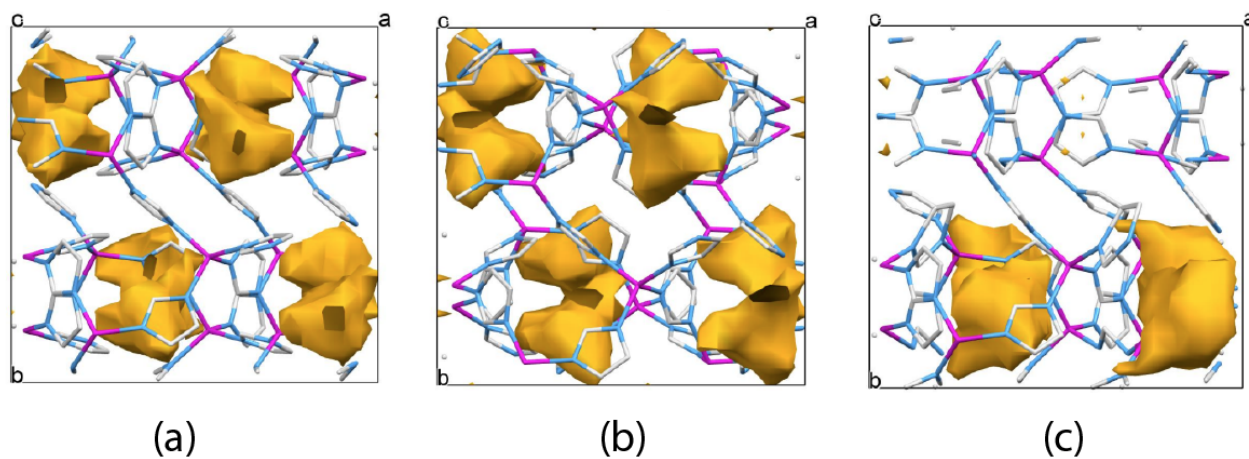


Fig. S9. (a) DFT optimized structure where the solvent accessible volume (SAV) is represented by the yellow surfaces. (b) Increase of SAV by 2~3% due to the 0.2 THz soft mode. (c) Coalescence of adjacent SAV at 1 THz ('gate-opening' mode) to yield further raise in the SAV.

8 Animations of ZIFs Lattice Dynamics

Web links to simulations calculated using Density Functional Theory (DFT), by applying the CRYSTAL14 code [14].

ZIF-4:

FIG.4a - Soft mode at 0.2 THz

<http://www.eng.ox.ac.uk/tan/thz-anim/ZIF4SoftModeAnimA.gif>

FIG.4b - Gate-opening mechanism at ~1 THz

<http://www.eng.ox.ac.uk/tan/thz-anim/ZIF4GateOpeningAnimB.gif>

ZIF-7:

FIG.5a - Soft mode at 0.652 THz

<http://www.eng.ox.ac.uk/tan/thz-anim/ZIF7SoftModesAnimA.gif>

FIG.5b - Breathing and shearing mechanisms at 0.654 THz

<http://www.eng.ox.ac.uk/tan/thz-anim/ZIF7BreathingShearingAnimB.gif>

FIG.5c - Breathing mechanism at 1.47 THz

<http://www.eng.ox.ac.uk/tan/thz-anim/ZIF7BreathingAnimC.gif>

ZIF-8:

FIG.6a - Soft mode at 0.57 THz

<http://www.eng.ox.ac.uk/tan/thz-anim/ZIF8SoftModeAnimA.gif>

FIG.6b - Shear mechanism at 0.65 THz

<http://www.eng.ox.ac.uk/tan/thz-anim/ZIF8ShearModeAnimB.gif>

FIG.6c - Gate-opening mechanism at 1 THz

<http://www.eng.ox.ac.uk/tan/thz-anim/ZIF8GateOpeningAnimC.gif>

9 References

1. Bennett, T.D., et al., *Structure and properties of an amorphous metal-organic framework*. Phys. Rev. Lett., 2010. **104**(11): 115503.
2. Zhao, P., et al., *Phase transitions in zeolitic imidazolate framework 7: The importance of framework flexibility and guest-induced instability*. Chem. Mater., 2014. **26**(5): 1767.
3. Park, K.S., et al., *Exceptional chemical and thermal stability of zeolitic imidazolate frameworks*. Proc. Natl. Acad. Sci. USA, 2006. **103**(27): 10186.
4. Tan, J.C., T.D. Bennett, and A.K. Cheetham, *Chemical structure, network topology, and porosity effects on the mechanical properties of zeolitic imidazolate frameworks*. Proceedings of the National Academy of Sciences of the United States of America, 2010. **107**(22): 9938.
5. <http://www.ccdc.cam.ac.uk>.
6. Moggach, S.A., T.D. Bennett, and A.K. Cheetham, *The effect of pressure on zif-8: Increasing pore size with pressure and the formation of a high-pressure phase at 1.47 gpa*. Angew. Chem. Int. Ed., 2009. **48**(38): 7087.
7. Colognesi, D., et al., *Tosca neutron spectrometer: The final configuration*. Appl. Phys. A-Mater., 2002. **74**: S64.
8. Dowden, Z.A., et al., *The tosca incoherent inelastic neutron spectrometer: Progress and results*. Physica B, 2000. **276**: 98.
9. Parker, S.F., et al., *Tosca: A world class inelastic neutron spectrometer*. Physica B, 1997. **241**: 154.
10. Cinque, G., et al., *Multimode infrared imaging and microspectroscopy (miriam) beamline at diamond*. Synchrotron Radiation News, 2011. **24**(5): 24.
11. *Handbook of vibrational spectroscopy*, ed. J.M. Chalmers and P.R. Griffiths. Vol. 1.
12. Perdew, J.P., K. Burke, and M. Ernzerhof, *Generalized gradient approximation made simple*. Physical Review Letters, 1996. **77**(18): 3865.
13. Grimme, S., *Semiempirical gga-type density functional constructed with a long-range dispersion correction*. J. Comput. Chem., 2006. **27**(15): 1787.
14. Dovesi, R., et al., *Crystal14: A program for the ab initio investigation of crystalline solids*. Int. J. Quantum Chem., 2014. **114**(19): 1287.
15. Tan, J.C., et al., *Exceptionally low shear modulus in a prototypical imidazole-based metal-organic framework*. Phys. Rev. Lett., 2012. **108**(9): 095502.
16. Broyden, C.G., *The convergence of a class of double-rank minimization algorithms 1. General considerations*. IMA Journal of Applied Mathematics, 1970. **6**(1): 76.
17. Broyden, C.G., *The convergence of a class of double-rank minimization algorithms: 2. The new algorithm*. IMA Journal of Applied Mathematics, 1970. **6**(3): 222.
18. Fletcher, R., *A new approach to variable metric algorithms*. Computer Journal, 1970. **13**(3): 317.

19. Goldfarb, D., *A family of variable-metric methods derived by variational means*. Mathematics of Computation, 1970. **24**(109): 23.
20. Shanno, D.F., *Conditioning of quasi-newton methods for function minimization*. Mathematics of Computation, 1970. **24**(111): 647.
21. Noel, Y., et al., *Polarization properties of zno and beo: An ab initio study through the berry phase and wannier functions approaches*. Phys. Rev. B, 2001. **65**(1).
22. Dovesi, R., et al., *Crystal14 user's manual, university of torino, torino, 2014*.
23. Zhou, W., et al., *Quasi-free methyl rotation in zeolitic imidazolate framework-8*. J. Phys. Chem. A, 2008. **112**(49): 12602.
24. Ramirez-Cuesta, A.J., *Aclimax 4.0.1, the new version of the software for analyzing and interpreting ins spectra*. Comput. Phys. Commun., 2004. **157**(3): 226.
25. Champion, D., J. Tomkinson, and G. Kearley, *A-climax: A new ins analysis tool*. Appl. Phys. A-Mater., 2002. **74**: S1302.
26. Frisch, M.J., et al., *Gaussian 09, revision b.01, 2009*, Gaussian, Inc.: Wallingford, CT, USA.
27. Møller, C. and M.S. Plesset, *Note on an approximation treatment for many-electron systems*. Physical Review, 1934. **46**(7): 618.
28. Kendall, R.A., T.H. Dunning, and R.J. Harrison, *Electron affinities of the first - row atoms revisited. Systematic basis sets and wave functions*. The Journal of Chemical Physics, 1992. **96**(9): 6796.
29. Sadlej, J., A. Jaworski, and K. Miaskiewicz, *A theoretical-study of the vibrational-spectra of imidazole and its different forms*. Journal of Molecular Structure, 1992. **274**: 247.
30. Sundaraganesan, N., et al., *Comparison of experimental and ab initio hf and dft vibrational spectra of benzimidazole*. Spectrochim Acta A Mol Biomol Spectrosc, 2007. **67**(3-4): 628.
31. Carter, D.A. and J.E. Pemberton, *Raman spectroscopy and vibrational assignments of 1- and 2-methylimidazole*. Journal of Raman Spectroscopy, 1997. **28**(12): 939.